Trilateral Flash Cycle for efficient low-temperature solar heat harvesting- A case study.

Anastasios Skiadopoulos[a], Christina Antonopoulou[b], Konstantinos Atsonios[c], Panagiotis Grammelis[d], Apostolos Gkountas[e], Panteleimon Bakalis[f], George Kosmadakis[g], and Dimitris Manolakos[h]

[a] Agricultural University of Athens, Athens, Greece, tskiado@aua.gr, CA
[b] Centre of Research and Technology Hellas, Athens, Greece, antonopoulou@certh.gr
[c] Centre of Research and Technology Hellas, Athens, Greece, atsonios@certh.gr
[d] Centre of Research and Technology Hellas, Athens, Greece, grammelis@certh.gr
[e] Psyctotherm SME, Piraeus, Greece, agountas@psyctotherm.gr
[f] Psyctotherm SME, Piraeus, Greece, pbakalis@psyctotherm.gr
[g] Ricreation IKE, Agia Paraskevi, Greece, gkosmad@ipta.demokritos.gr
[h] Agricultural University of Athens, Athens, Greece, dman@aua.gr

Abstract:

In this work, the annual performance of a solar thermal power system in Greece is numerically studied. The system consists of a field of Evacuated Tube Collectors and a Trilateral Flash Cycle engine. The main target of this study is to assess the potential of the Trilateral Flash Cycle, a promising higher efficiency alternative to the Organic Rankine Cycle, for solar energy exploitation. The effects of the solar irradiance, the temperature of the heat source, and the flashing efficiency on the total solar energy conversion efficiency are monitored. The economics of the system is preliminarily studied taking into account its scale and the anticipated annual power output. Simulations indicate that the combined Solar-Trilateral Flash Cycle system can achieve an average annual total solar energy conversion efficiency of 5%, outperforming a Solar-Organic Rankine Cycle system of similar architecture at the examined location. It is demonstrated that the efficiency of the Trilateral Flash Cycle engine is highly dependent on the quality of the Working Fluid at the onset of expansion, and the operating pressure ratio. Moreover, the Trilateral Flash Cycle can achieve a thermal efficiency of up to 11%. The Levelized Cost of Electricity of the power system is estimated to lie in the region of 0.26 - 0.32 €/kWh, based on its scale, indicating that it may be a competitive solution for solar energy exploitation.

Keywords:

Solar Energy; Trilateral Flash Cycle; Two-Phase Expansion; Evacuated Tube Collectors; Solar Efficiency; Thermal Efficiency.

1. Introduction

Solar energy presents a huge potential for green power generation, especially in locations with low to middle latitudes, and it may be efficiently exploited by solar thermal power systems. In these systems, solar thermal collectors generate heat that is utilized for power production by a heat-to-power conversion technology. Several types of solar thermal collectors, with different ranges of applications each, have been developed [1], and they are currently considered to be at a mature technological level [2]. These collectors provide heat at rather low temperatures (<400°C), a range where the traditional water-steam Rankine power cycles of centralized power stations cannot operate efficiently. The overall solar energy conversion efficiency of solar thermal power systems depends on the collectors' efficiency and the thermal efficiency (heat-to-power ratio) of the power generation technology. Bottoming power cycles are a widely applied solution for the efficient exploitation of low-temperature heat, with the Organic Rankine Cycle (ORC) indicated as a robust solution because of its flexible design, low maintenance cost, and nearly unsupervised operation [3].

Many works have been published in the literature (e.g. [4–7]) assessing the potential and efficiency of the ORC, both numerically and experimentally, with different heat sources. The main drawback of the ORC is the drop in its thermal efficiency at lower heat source temperatures. Several studies have been published in the literature (e.g. [8]) aiming to identify the causes for this efficiency drop. The consensus is that the energy losses in the ORC are mainly ought to the isothermal vaporization process of the Working Fluid (WF) at the evaporator of the cycle. During this process, the temperature of the WF remains constant while the temperature of the Heat Transfer Fluid (HTF) drops, leading to a sub-optimal match between the finite heat source and the WF. The optimal match between the heat source and the WF may be accomplished when the power cycle obtains

https://doi.org/10.52202/069564-0010

a trilateral shape [8], where the vaporization of the WF is omitted. One such possible high-efficiency power cycle variant is the Trilateral Flash Cycle (TFC), initially conceptualized by Smith et al. [9].

The TFC consists of the same components as the ORC but the WF enters the power generator in the saturated liquid state, or partially evaporated in the generalized version of the TFC, where it undergoes two-phase expansion, also known as flashing. The TFC is not technologically mature, mainly because of the lack of fundamental knowledge about the complex flashing phenomenon in the expander. Only a few experimental works ([10–12]) have been performed in two-phase expansion until now, with the quality of the WF at the onset of expansion identified as the most significant factor affecting the efficiency of the two-phase expander. Higher vapor qualities result in increased efficiencies of the two-phase expansion, which can reach 80% [11]. Furthermore, only a few numerical models [13–16] have been developed to simulate two-phase expansion, all of which simulate flashing in twin-screw expanders. In the work of Skiadopoulos et al. [16], a semi-empirical thermodynamic low-order model was developed to simulate two-phase expansion in twin-screw expanders. In this model, a segmental approach is applied to monitor the evolution of flashing in the expansion chamber. Moreover, the liquid and vapor phases are assumed to be in thermal non-equilibrium and a two-fluid model approach is followed for the formulation of the governing equations.

The purpose of this work is to assess the performance of a small-scale solar thermal power system in Athens, Greece, driven by low-temperature solar heat, which is provided by a field of Evacuated Tube Collectors (ETCs), and exploited by a TFC bottoming power cycle. To the best of the authors' knowledge, this is the first work in the literature systematically investigating the promising TFC power cycle for solar heat exploitation. The ETCs are selected for the system, because of their increased efficiency in comparison to Flat Plate Collectors, which are typically preferred for small-scale systems because of their lower cost. An integrated numerical tool simulating the annual performance of the combined Solar-TFC system is developed, in the software environment of Matlab (R2022b). The numerical model utilizes meteorological data for the installation site, provided by the National Observatory of Athens. Another novel feature of this work is that in TFC modeling, the performance of the two-phase expander, under varying operating conditions, is accurately monitored, by applying the novel thermodynamic low-oder model developed by Skiadopoulos et al. [16]. This approach in two-phase expansion modeling comes to fill a gap in the relevant literature since several theoretical works studying the performance of the TFC have been published, but the two-phase expander is usually treated as a black box with isentropic efficiencies achieved in the dry-vapor region [17,18]. R245fa is selected as the WF of the TFC, because it has been tested as a WF in Solar-ORC systems, numerically and experimentally, demonstrating very good thermodynamic behavior within the range of temperature and operating pressure ratios of low-temperature solar systems [6,7].

This paper is organized as follows. In Section 2, the architecture of the integrated system, the governing equations, and the numerical methodology are presented in detail. Moreover, the methodology for the economic assessment of the Solar-TFC system is presented. In Section 3, the performance of the ETCs, the TFC, and the integrated system are investigated in detail. Thereafter, the annual electricity output of the unit and the achievable total solar energy conversion efficiency, along with the thermal efficiency of the TFC and the second law efficiency of the Solar-TFC system, under optimal operating conditions, throughout the year are estimated. Finally, a short economic analysis of the Solar-TFC system is presented. General conclusions and remarks are presented in Section 4.

2. Materials and Methods

2.1. Description of the Solar-TFC system

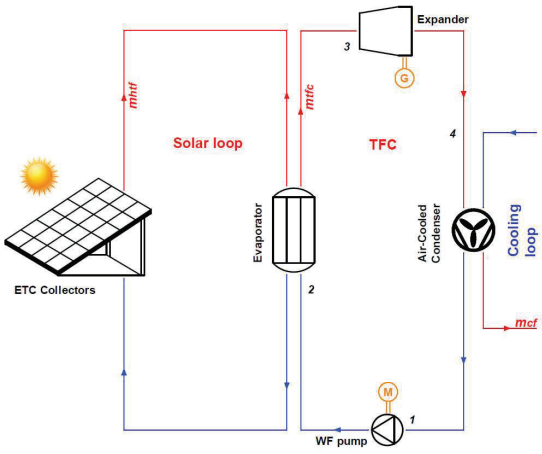

Figure 1. Schematic layout of the Solar-TFC system.

https://doi.org/10.52202/069564-0010

A schematic layout of the modeled Solar-TFC system is presented in Figure 1. The unit operates in HTF mode, i.e. solar thermal energy is transferred from the field of the ETC to the evaporator of the TFC through an HTF. In the evaporator of the TFC, the WF is heated up, at high pressure, reaching the state of the saturated liquid or the two-phase mixture. Thereafter, it flows through the two-phase expander, where flashing occurs and power is generated. The two-phase mixture at the expander's discharge dissipates heat to the environment through the air-cooled condenser. Finally, the WF is pumped to the operating pressure of the evaporator, and the power cycle starts anew. The thermodynamic states of the WF in the TFC (numbered 1÷4) are presented in Figure 1. Details regarding the thermodynamic processes of the WF in the TFC are given in Section 2.2.2. The thermodynamic properties of the HTF, the WF, and the CF are calculated by utilizing the CoolProp library [19] wrapper for Matlab.

2.2. Modeling

2.2.1. ETC collectors

The Thermomax DF 100 30, developed by Kingspan Thermomax, ETCs are selected for the solar field. The technical specifications of the selected ETCs are listed in Table 1. The inclination angle β is selected to maximize the annually absorbed solar energy at the installation site [7]. The values of T_{min} and T_{max} are typical of low-temperature solar power systems, ensuring low thermal losses towards the ambient, and, at the same, subcritical operation of the power cycle (taking into consideration that the critical temperature of R245fa is equal to 154 °C). Based on T_{max}, H_2O pressurized at 4 bar, to avoid boiling in the solar loop, is selected as the HTF. Finally, $\dot{m}_{htf}/A_{col}$ takes the average value of the recommended, by the collectors' developer, mass flowrate range for the solar cooling loop.

Table 1. Technical specifications of the ETCs.

Parameter	Symbol	Value [Units]
Aperture area	A_{ap}	3.228 [m^2]
Optical efficiency at normal incidence	η_o	0.779 [-]
First-order losses coefficient (based on A_{ap})	a_1	1.07 [W/m^2-K]
Second-order losses coefficient (based on A_{ap})	a_2	0.0135 [W/m^2-K^2]
Heat Transfer Fluid	HTF	H_2O [-]
Collector Area- Specific HTF flowrate	$\dot{m}_{htf}/A_{col}$	$2.95 \cdot 10^{-2}$ [kg/m^2-s]
Inclination angle	β	32 [°]
Minimum collectors' temperature	T_{min}	80 [°C]
Maximum collectors' temperature	T_{max}	130 [°C]

The thermal efficiency η_{col} of the collectors is calculated by Eq. (1). This empirical formula is applied commonly in solar collectors' modeling because the value of the coefficients η_o, a_1, and a_2 are available from the collectors' certification experiments.

$$\eta_{col} = \eta_o - a_1 \cdot \frac{(T_m - T_{amb})}{G_{tot}} - a_2 \cdot \frac{(T_m - T_{amb})^2}{G_{tot}} \quad (1)$$

In Eq. (1) G_{tot} is the total solar irradiance on the collectors' surface, T_m is their average temperature, and T_{amb} is the ambient temperature. The heat gain $\dot{Q}_{col}$ of the collectors is then given by Eq. (2), where A_{col} is the total area of the collectors.

$$\dot{Q}_{col} = \eta_{col} \cdot A_{col} \cdot G_{tot} \quad (2)$$

A common assumption in solar power system simulations is that T_m is equal to the average temperature of the HTF flowing in the solar loop. This assumption is expressed by Eq. (3), where $T_{htf,in}$ and $T_{htf,out}$ are the temperatures of the HTF flowing in and out of the solar cooling loop, respectively.

$$T_m = \frac{T_{htf,in} + T_{htf,out}}{2} \quad (3)$$

During steady-state operation of the Solar-TFC system, and if the heat losses at the HTF circuit are assumed negligible, $\dot{Q}_{col}$ is equal to the heat transfer rate $\dot{Q}_{ev}$ to the evaporator of the TFC engine. $\dot{Q}_{ev}$, on the HTF side, is given by Eq. (4), with $c_{p,htf}$ representing the specific heat capacity, under constant pressure, of the HTF, calculated at T_m.

$$\dot{Q}_{ev} = \dot{m}_{htf} \cdot c_{p,htf}\left(T_{htf,out} - T_{htf,in}\right) \quad (4)$$

The total irradiance G_{tot} on the inclined surface of the collectors is given by Eq. (5), where G_b and G_d are the beam irradiance normal on the collectors, and the diffuse irradiance, respectively (ground-reflected irradiance is not considered).

$$G_{tot} = G_b + G_d \quad (5)$$

G_b is calculated based on the available meteorological data at the installation site. Specifically, G_b is given by Eq. (6), where G_h is the beam irradiance on a horizontal surface, and R_b is the beam radiation tilt factor.

$$G_b = G_h \cdot R_b \tag{6}$$

R_b is given at each instance by applying Eq. (7), where L is the local latitude, δ the solar declination, and hr the hour angle. Detailed methodology concerning the calculation of R_b is presented by Kalogirou [20].

$$R_b = \frac{\sin(L-\beta)\cdot\sin(\delta) + \cos(L-\beta)\cdot\cos(\delta)\cdot\cos(hr)}{\sin(L)\cdot\sin(\delta) + \cos\cdot(L)\cdot\cos(\delta)\cdot\cos(hr)} \tag{7}$$

2.2.2. TFC

A qualitative Temperature- Entropy (T-s) diagram of the TFC power cycle with R245fa as the WF is presented in Figure 2, where the thermodynamic processes undergone by the WF, the HTF, and the Cooling Fluid (CF) are drawn. The thermodynamic processes of the TFC are the following:

- 1→2: Adiabatic pumping
- 2→3: Heat absorption in the evaporator at constant pressure p_{ev}
- 3→4: Adiabatic expansion in the two-phase expander
- 4→1: Heat rejection in the condenser at constant pressure p_{con}

The WF is sub-cooled at the suction port of the pump to prevent cavitation. Heat is transferred to the evaporator of the TFC engine by the HTF of the solar cooling loop, leading to a drop in its temperature from $T_{htf,out}$ to $T_{htf,in}$. Heat is dissipated from the TFC in the condenser, resulting in the temperature rise of the CF from $T_{cf,in}$ to $T_{cf,out}$. Herein, the term TFC is generalized to engulf the power cycle architectures where the WF at the onset of expansion can be in a state ranging from saturated liquid to saturated vapor.

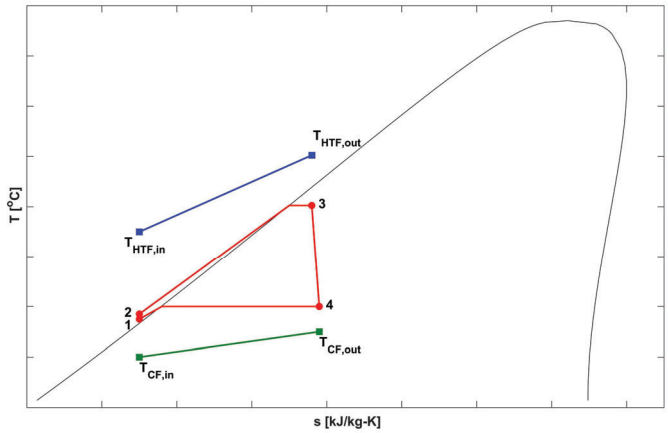

Figure 2. T-s diagram of the TFC with R245fa as the WF.

The parameters, along with their values and symbols, for the numerical modeling of the TFC are listed in Table 2. Assuming negligible heat losses at the TFC evaporator, $\dot{Q}_{ev}$ will be equal to the heat absorbed by the WF of the TFC, equality expressed by Eq. (8), where $\dot{m}_{wf}$ is the mass flowrate of the WF, whereas h_3 and h_2 are the specific enthalpies of the WF at thermodynamic states 2 and 3 of the power cycle, respectively.

$$\dot{Q}_{ev} = \dot{m}_{wf} \cdot (h_3 - h_2) \tag{8}$$

Table 2. Modeling parameters of the TFC cycle.

Parameter	Symbol	Value [Units]
Pinch point temperature difference at the evaporator	PP_{ev}	5 [°C]
Pinch point temperature difference at the condenser	PP_{con}	5 [°C]
Pump isentropic efficiency	$\eta_{pu,is}$	0.75 [-]
Working Fluid	WF	R245fa
Cooling Fluid	CF	Air [-]
Temperature rise of the Cooling Fluid	ΔT_{cf}	10 [°C]
Working fluid sub-cooling at pump suction	ΔT_{sub}	5 [°C]

https://doi.org/10.52202/069564-0010

The temperature T_4 of the WF at the onset of condensation is derived from PP_{con}, as in Eq. (9)

$$T_4 = T_{cf,out} + PP_{con} \tag{9}$$

where $T_{cf,out}$ is the temperature of the CF at the outlet of the condenser's cooling loop, given by Eq. (10). In Eq. (10), $T_{cf,in}$ is the temperature of the CF at the inlet of the cooling loop, equal to T_{amb} for the modeled case of the air-cooled condenser in this work.

$$T_{cf,out} = T_{cf,in} + \Delta T_{cf} \tag{10}$$

After applying Eq. (9), p_{con} is readily calculated, as the saturation pressure of the WF at T_4. The coupling between the TFC and the solar cooling cool is accomplished by PP_{ev}, as expressed by Eq. (11), where $T_{htf,pr}$ is the temperature of the HTF at the end of the preheating stage, and $T_{sat,wf}(p_{ev})$ is the saturation temperature of the WF at p_{ev}. In the ideal trilateral cycle, $T_{htf,pr}$ becomes equal to $T_{htf,out}$.

$$T_{htf,pr} = T_{sat,wf}(p_{ev}) + PP_{ev} \tag{11}$$

Equation (12) must be satisfied along with Eq. (8). In Eq. (12), $\dot{Q}_{pr}$ is the heat transfer rate from the HTF to the WF during the preheating stage, and $h_{l,sat}(p_{ev})$ is the enthalpy of the saturated liquid at p_{ev}.

$$\dot{Q}_{pr} = \dot{m}_{wf} \cdot \left(h_{l,sat}(p_{ev}) - h_2\right) = \dot{m}_{htf} \cdot c_{p,htf} \cdot \left(T_{htf,pr} - T_{htf,in}\right) \tag{12}$$

The numerical procedure for the determination of $\dot{m}_{wf}$ and p_{ev}, for a desired quality x_3 of the two-phase mixture at the onset of expansion is as follows. The value of p_{ev} is varied iteratively in a stepwise manner. For a guess intermediate value of p_{ev}, the saturation temperature $T_{sat,wf}(p_{ev})$ of the WF is calculated, and, subsequently, $T_{ht\ ,pr}$ is derived by applying Eq. (11). Thereafter, two values for $\dot{m}_{wf}$ are calculated by simultaneously applying Eqs. (8) and (12). The iterations on p_{ev} terminate when the two values of $\dot{m}_{wf}$ converge.

After the values of $\dot{m}_{wf}$ and p_{ev} have been determined, the thermodynamic low-order two-phase expansion model (details about the methodology applied in the two-phase expansion model can be found in Ref. [16]), is run. The outcome of the simulation is the rotational speed of the expander for the given mass flowrate, and the specific enthalpy h_4 of the WF at the discharge port. Thereafter, the isentropic efficiency $\eta_{ex,is}$ of expansion is calculated by Eq. (13), where $h_{4,is}$ is the specific enthalpy of the WF corresponding to an isentropic expansion from state 3 at p_{ev} to p_{con}.

$$\eta_{ex,is} = \frac{h_3 - h_4}{h_3 - h_{4,is}} \tag{13}$$

The power $\dot{w}_{ex}$ generated by the two-phase expander is given by Eq. (14)

$$\dot{w}_{ex} = \dot{m}_{wf} \cdot (h_3 - h_4) \tag{14}$$

whereas the power $\dot{w}_{pu}$ absorbed by the pump is calculated by Eq. (15), in which h_1 is the specific enthalpy of the WF at its suction.

$$\dot{w}_{pu} = \dot{m}_{wf} \cdot (h_2 - h_1) \tag{15}$$

h_2 is derived by applying the formula for the isentropic efficiency $\eta_{pu,is}$ of the pump, as in Eq. (16).

$$\eta_{pu,is} = \frac{h_{2,is} - h_1}{h_2 - h_1} \tag{16}$$

In Eq. (16), $h_{2,is}$ is the specific enthalpy of the WF corresponding to its isentropic pumping from state 1 at p_{con} to p_{ev}. The thermal efficiency η_{th} of the TFC is given by Eq. (17), where $\dot{w}_{net}$ is the net power generated by the TFC engine.

$$\eta_{th} = \frac{\dot{w}_{net}}{\dot{Q}_{ev}} = \frac{\dot{w}_{ex} - \dot{w}_{pu}}{\dot{Q}_{ev}} \tag{17}$$

The heat transfer rate $\dot{Q}_{con}$ at the condenser is calculated by Eq. (18), leading to the evaluation of the necessary mass flowrate $\dot{m}_{cf}$ of the CF. In Eq. (18) $c_{p,cf}$ is the specific heat capacity, under constant pressure, of the CF.

$$\dot{Q}_{con} = \dot{m}_{wf} \cdot (h_4 - h_1) = \dot{m}_{cf} \cdot c_{p,cf} \cdot \Delta T_{cf} \tag{18}$$

2.2.3. Solar-TFC system

At any operating instance of the Solar-TFC system, the overall solar energy conversion efficiency η_{tot} is given by Eq. (19).

$$\eta_{tot} = \eta_{col} \cdot \eta_{th} = \frac{\dot{Q}_{col}}{A_{col} G_{tot}} \cdot \frac{\dot{w}_{net}}{\dot{Q}_{ev}} = \frac{\dot{w}_{net}}{A_{col} \cdot G_{tot}} \quad (19)$$

Moreover, the exergy efficiency η_{II} of the unit is given by Eq. (20)

$$\eta_{II} = \frac{\dot{w}_{net}}{\left(1 - \frac{T_{amb}}{T_{sol}}\right) A_{col} \cdot G_{tot}} \quad (20)$$

where T_{sol} is the solar reference temperature, taken equal to 5770 K for this work [7].

The average thermal efficiency $\eta_{th,av}$ of the TFC engine, and the average solar energy conversion efficiency $\eta_{tot,av}$ and average exergy efficiency $\eta_{II,av}$ of the combined unit over a period are calculated by integrating Eqs. (17), (19), and (20), respectively.

2.3. Economic analysis

The economics of the Solar-TFC system is assessed by evaluating the Levelized Cost of Electricity ($LCOE$), an estimation of the average cost that the owner-operator of the system will have to pay for every kWh produced during its anticipated lifetime N. $LCOE$ is given by Eq. (21)

$$LCOE = \frac{C_{inv} + \sum_{i=1}^{N} \frac{M}{(1+i)^r}}{\sum_{i=1}^{N} W} \quad (21)$$

where C_{inv} is the total initial investment cost, W is the total electricity produced at year i, M is the annual maintenance cost at year i, and r is the annual discount rate. In this work, it is assumed that W, as well as M and r remain constant throughout N. C_{inv} is given by Eq. (22), where sc_{tfc} and sc_{col} are the specific costs of the TFC and the ETC collectors, respectively, whereas P_{tfc} is the nominal electric capacity of the TFC.

$$C_{inv} = sc_{tfc} \cdot P_{tfc} + sc_{col} \cdot A_{col} \quad (22)$$

The values of the parameters for the economic analysis are listed in Table 3. Analysis concerning the estimation of sc_{tfc}, based on the nominal capacity of the TFC is presented in Section 3.3.3.

Table 3. Parameters of the economic analysis.

Parameter	Symbol	Value [Units]
Lifetime	N	20 [yr]
Annual discount rate	r	5 [%] [7,21]
Annual maintenance cost	M	$0.01 C_{inv}$ [€]
Specific cost of collectors	sc_{col}	260 [€/m^2] [6]

3. Results & Discussion

3.1. Solar field

The performance of the solar field is assessed based on the achievable values for η_{col} as a function of G_{tot}, T_{amb}, and T_m for a clear-sky day at the installation site. The variation of G_{tot}, G_d, and T_{amb} from sunrise to sunset, with an hourly time step, as a function of solar time for the reference day is presented in Figure 3. The fluctuation of η_{col} and $\dot{Q}_{ev}/A_{col}$ versus solar time for the reference day and different desired operating temperatures T_m is presented in Figure 4. It is assumed that the TFC engine operates when the temperature of the collectors reaches the desired value of T_m, and, thereafter, T_m remains constant for as long as possible, based on the values of G_{tot} and T_{amb}. Therefore, during the heating up of the collectors, it is assumed that the solar irradiance is exploited initially only to increase T_m ($\dot{Q}_{ev} = 0$) until its desired value has been reached. Subsequently, (and for as long as $\dot{Q}_{col} > 0$) all the heat gain $\dot{Q}_{col}$ is delivered to the TFC engine ($\dot{Q}_{col} = \dot{Q}_{ev}$), and T_m is kept constant. When $\dot{Q}_{col} < 0$, the collectors are cooled down, and the operation of the TFC engine stops.

After sunrise, the temperature of the collectors begins to increase, with a gradual drop in η_{col} because the temperature difference $T_m - T_{amb}$ rises and the heat losses towards the ambient are increased. After the desired operating temperature T_m has been reached, η_{col} rises as G_{tot} and T_{amb} increase, and it drops gradually after solar noon. The maximum values of η_{col} and $\dot{Q}_{ev}/A_{col}$ (while the TFC engine is operating), equal to 0.664 and 676.84, respectively, are obtained for T_m equal to 80 °C. Increasing T_m reduces η_{col} and $\dot{Q}_{ev}/A_{col}$ because the heat losses towards the ambient are also higher. However, reducing T_m may harm η_{th}, as the

https://doi.org/10.52202/069564-0010

operating pressure ratio of the TFC will drop. The effect of T_m, along with other identified crucial parameters, on the efficiency of the TFC is described in detail in Section 3.2.

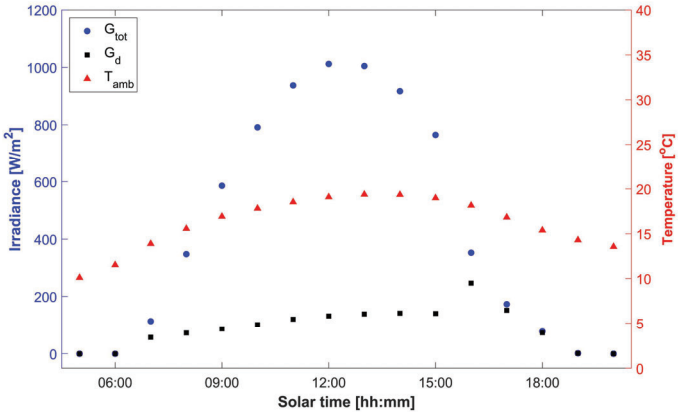

Figure 3. Irradiance on ETC collectors and T_{amb} as a function of solar time on a clear-sky spring day.

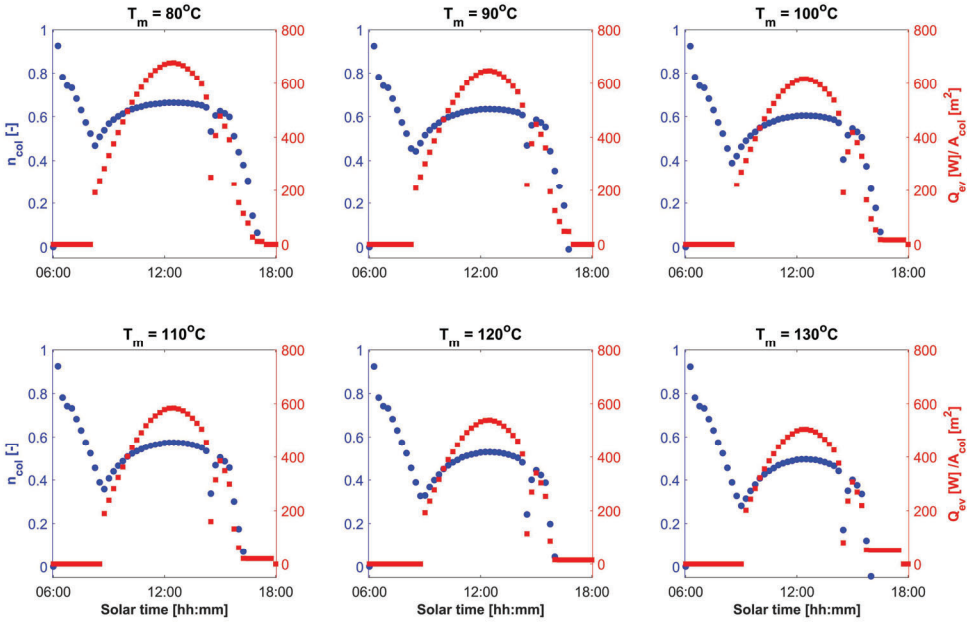

Figure 4. η_{col} and $\dot{Q}_{ev}/A_{col}$ as a function of solar time for different values of T_m.

3.2. TFC

The performance of the TFC is assessed based on its efficiency at solar noon, when the irradiance on the collectors is maximized, of the reference day presented in Section 3.1. The value of η_{th} depends on the isentropic efficiency $\eta_{ex,is}$ of the two-phase expansion, which, in turn, is directly related to x_3 and T_m, as can be seen in Figure 5. Low vapor quality at the suction port of the two-phase expansion leads to very low values of $\eta_{ex,is}$. This is attributed to the increased pressure losses at suction and the increased mass flowrates $\dot{m}_{wf}$ of the WF, which cannot be accommodated by the modeled expander [11,16]. Furthermore, as T_m and x_3 vary, the deviation of the WF volume ratio from the built-in volume ratio of the two-phase expander varies as well. For every T_m there is a value of x_3 for which an optimal match between the two values is obtained, and the over-under expansion losses are minimized.

Increasing $\eta_{ex,is}$ has an obvious positive effect on η_{th}, and values as high as 0.11 can be achieved. The variation of $\eta_{ex,is}$ and η_{th} with x_3, for the range of values for T_m, indicates that the optimal operating point of

the unit lies always within the two-phase region, as their values are systematically reduced towards the saturated vapor state.

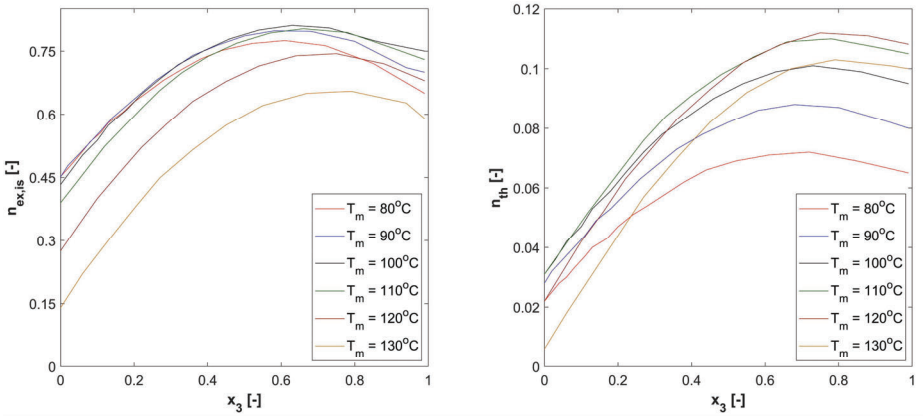

Figure 5. $\eta_{ex,is}$ and η_{th} versus x_3 for different values of T_m.

3.3. Solar-TFC

3.3.1. Performance optimization

The analysis presented in Sections 3.1 and 3.2 highlighted that there are two degrees of freedom, i.e. T_m and x_3, in the Solar-TFC system, the determination of which leads to the maximization of η_{tot} for given irradiance and T_{amb} values. The system of Eqs. presented in Sections 3.1, 3.2, and 3.3 is formulated in Matlab, wherein a native genetic algorithm, which leads to the determination of the global optimum, is applied aiming to maximize η_{tot}, with T_m and x_3 the iteration variables. The optimization problem is solved throughout the year with a fifteen minute interval.

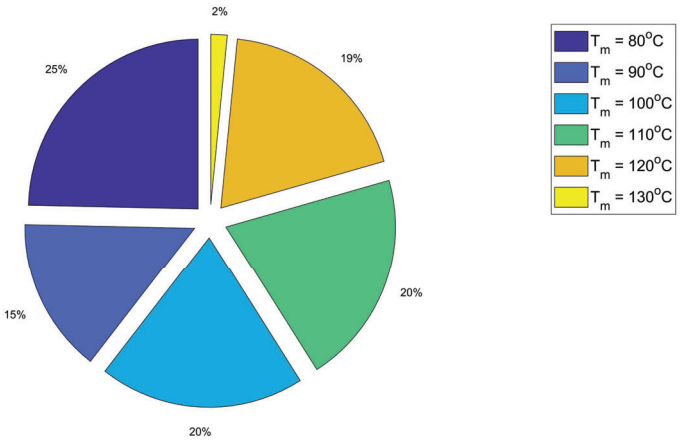

Figure 6. Frequency distribution of optimal T_m value per year.

The simulations reveal that the Solar-TFC system can be operational for a total of 2835 hours per year in Athens. The frequency distribution of the optimal T_m on the annual basis is presented in Figure 6. It can be deduced that T_{min} is the most frequent optimal operating temperature of the collectors. This is justified since an annual optimization is undertaken, and days with low values of irradiance and T_{amb} are also considered. On the other hand, it must be stressed that it is optimal to operate the system at T_{max} for only about 2% of the unit's operating time around the year. This is because, as analyzed in Sections 3.1 and 3.2, the heat losses of the solar field towards the ambient are very high, and, at the same time, the efficiency of the TFC is rather low, because of low $\eta_{ex,is}$ values. T_{max} is optimal only in a few instances during summer, when $\dot{Q}_{ev}/A_{col}$ is maximized because of the high irradiance, and, T_{amb} is high enough to ensure a favorable WF volume ratio, and, therefore, an operating pressure ratio for the TFC. The variation of the optimal x_3 throughout the year is presented in Figure 7, and it ranges from 0.59 to 0.83. As analyzed in Section 3.2, high values of x_3 ensure satisfying $\eta_{ex,is}$, and, as a result, increased η_{th}, a finding consistent with experiments [11].

https://doi.org/10.52202/069564-0010

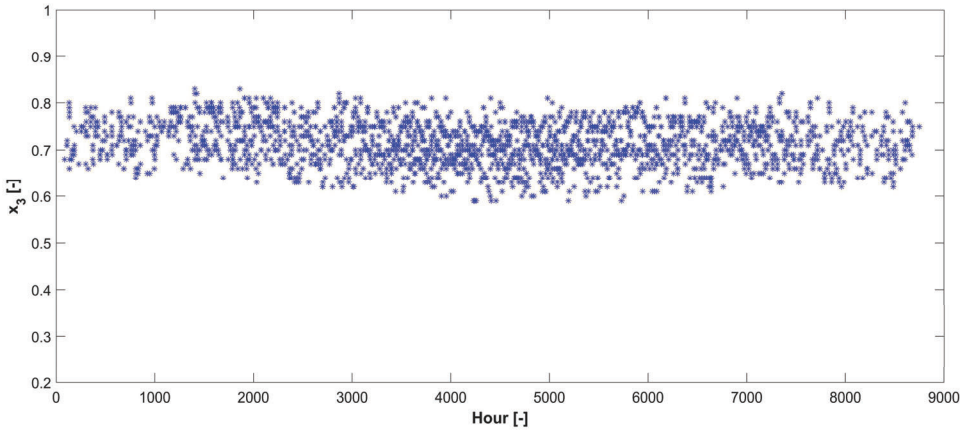

Figure 7. Optimal vapor quality x_3 at the suction port of the expander throughout the year.

3.3.2. Annual yield and efficiency

The total collectors' area- specific solar energy E_{sol}/A_{col} incident on the ETCs monthly, for the operational time of the Solar-TFC system, along with the average monthly $\eta_{tot,av}$ are presented in Figure 8.

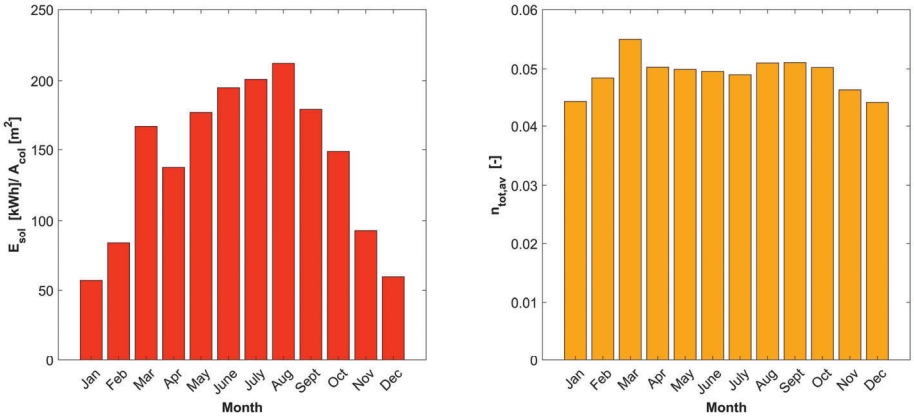

Figure 8. Monthly variation of E_{sol}/A_{col} and $\eta_{tot,av}$.

E_{sol}/A_{col} is maximized in August, however, the combined system is most efficient in solar energy harvesting during March. This can be explained as follows. The irradiance on the collectors may be higher during summer, but the utilization of an air-cooled condenser increases the condensation temperature and pressure (see Eqs. (9) and (10)), and the operating pressure ratio p_{ev}/p_{con} of the TFC is reduced, with adverse effects on the power generation potential. If the condensation temperature was kept constant throughout the year, it is expected that $\eta_{tot,av}$ would be higher in summer.

The average annual solar energy conversion efficiency $\eta_{tot,av}$ of the Solar-TFC system is equal to 0.05, which is substantially higher than the one estimated (0.03) for a small-scale Solar-ORC system at the installation site [6], which consists of the same ETCs and two scroll expanders, installed in series, as power generators. The monthly distribution of the total collectors' area-specific W/A_{col} electricity produced by the TFC, and the values of $\eta_{II,av}$ and $\eta_{th,av}$ are presented in Figure 9. The annual yield of electricity is equal to 86 kWh per m^2 of collectors, with an average $\eta_{th,av}$ equal to 0.10. This average annual efficiency is again higher than the calculated (0.089) from the simulations of the aforementioned small-scale Solar-ORC system at the same location, demonstrating the potential of the TFC for higher-efficiency solar thermal power systems. The annual average exergy efficiency $\eta_{II,av}$ is approximately 0.05, a value slightly lower than the one simulated for a small-scale Solar-ORC system with R245fa as the WF in Athens [7]. However, that unit utilizes Parabolic Trough Collectors, which achieve higher values of η_{col}, but are most costly.

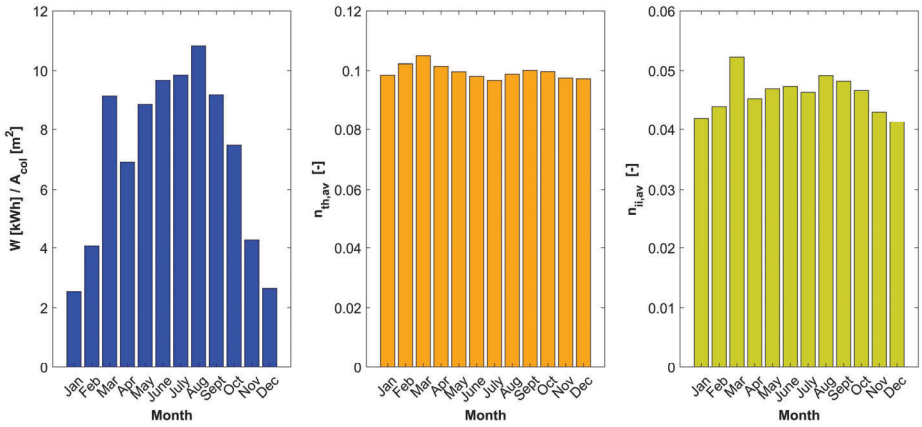

Figure 9. Monthly variation of W/A_{col}, $\eta_{th,av}$, and $\eta_{II,av}$.

3.3.3. Economic assessment

The economics of the Solar-TFC system is assessed by performing a parametric analysis, with A_{col} and sc_{tfc} the degrees of freedom. A_{col} implicitly determines the value of P_{tfc}. It is assumed that G_t, T_m, and T_{amb} are equal to 1000 W/m^2, 110 ^{o}C, 20 ^{o}C, respectively, at the design point of the unit. By applying Eq. (1), η_{col} is calculated and, assuming a gross value, i.e. neglecting $\dot{w}_{pu}$, of η_{th} equal to 0.08, the value of P_{tfc} may be readily calculated. Thereafter, sc_{tfc} is estimated based on the values of P_{tfc}, the nominal heat capacity, and the temperature of the heat source, according to the work of Braimakis et al. [22]. The values of P_{tfc} and sc_{tfc} as a function of A_{col} are listed in Table 4. It must be noted that the parametric values of A_{col} were selected to ensure that P_{tfc} lies within the operating nominal electric capacities of twin screw expanders [23].

$LCOE$ versus A_{col} is plotted in Figure 10. As A_{col} increases, $LCOE$ drops because sc_{tfc} is diminished. The estimated $LCOE$ values are considered competitive against the current electricity prices at the European Union, and also against the reported $LCOE$ values of Solar-ORC systems in the literature, that range between 0.25 and 0.95 €/kWh [6,7,24]. The penetration of the Solar-TFC system in the market could be further assisted in the future, considering the European policies to assist the participation of renewables in the energy mix and promote decentralized energy production.

Table 4. Parametric values of A_{col}, P_{tfc}, and sc_{tfc} at the Solar-TFC system design point.

A_{col} [m^2]	200	300	400	500	600
P_{tfc} [kW$_{el}$]	9	14	18	23	28
sc_{tfc} [€/kW$_{el}$]	4850	4300	3800	3300	3000

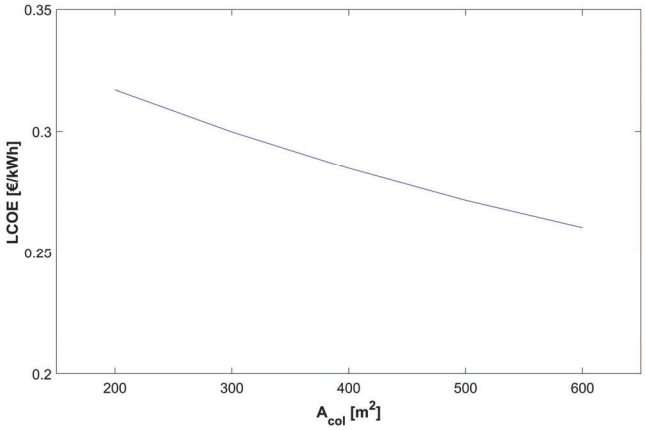

Figure 10. $LCOE$ as a function of A_{col}.

https://doi.org/10.52202/069564-0010

4. Conclusions

In the present work, the annual performance of a Solar-TFC power system located in Athens was numerically studied. The operation of the system was optimized throughout the year to maximize solar energy conversion efficiency. Particular attention was paid to the two-phase expansion efficiency, which mainly affects the thermal efficiency of the TFC, with flashing simulations indicating that higher vapor qualities (59-83%) of the WF at the onset of expansion have a positive effect on the power cycle performance. The numerical results indicated that 86 kWh of green power per m^2 of collectors can be generated by the Solar-TFC system annually, with the average solar energy conversion efficiency reaching 5%, higher than the one estimated for a Solar-ORC system with similar architecture in Athens. The average annual thermal efficiency of the TFC and exergy efficiency of the combined Solar-TFC system were calculated approximately equal to 10% and 5%, respectively.

The preliminary economic analysis of the Solar-TFC system demonstrated the potential of the TFC as a competitive replacement of the ORC for solar heat recovery. Indeed, $LCOE$ values in the range of 0.26 - 0.32 €/kWh can be anticipated for an operation reaching 20 years. The economics of the system is better as its size increases, because of the TFC engine's lower specific cost at higher capacities.

Concluding, the analysis presented in this work highlighted the potential of the TFC for efficient solar energy conversion, and its competitiveness compared to the ORC. However, it must be noted that additional research work is necessary for the TFC to reach a technologically mature level. This research work must mainly focus on the comprehension of the flashing phenomenon and the development of expanders that will operate efficiently in the two-phase region.

Acknowledgments

This research work was supported by the *Operational Programme Competitiveness, Entrepreneurship, and Innovation 2014-2020 (EPAnEK)*. (Project Number: T2EΔK-00351, Acronym: TRI-MAX).

Nomenclature

Symbols		**Subscripts**		II	Second Law
p	Pressure [bar]	in	Inlet	av	Average
T	Temperature [°C]	out	Outlet	ap	Aperture
A	Collectors' area [m^2]	is	Isentropic	sol	Solar
h	Specific enthalpy [kJ/kg]	ex	Expander	htf	Heat Transfer Fluid
s	Specific entropy [kJ/kg-K]	ev	Evaporator	wf	Working Fluid
G	Irradiance [W/m^2]	con	Condenser	cf	Cooling Fluid
c_p	Specific heat [kJ/kg-K]	sub	Subcooling	**Greek letters**	
$\dot{m}$	Mass flow rate [kg/s]	pr	Preheating	δ	Solar declination [°]
$\dot{w}$	Power [kW]	pu	Pump	η	Efficiency [-]
x	Vapor quality [-]	sat	Saturated	β	Inclination angle [°]
W	Electricity [kWh]	th	Thermal	α	Losses Coefficient [-]
$\dot{Q}$	Heat transfer rate [kW]	l	Liquid	**Abbreviations**	
C	Cost [€]	amb	Ambient	TFC	Trilateral Flash Cycle
r	Discount rate [%]	m	Mean	ETC	Evacuated Tube Collector
L	Latitude [°]	col	Collector	HTF	Heat Transfer Fluid
P	Nominal power [kW]	d	Diffuse	CF	Cooling Fluid
sc	Specific cost [€/m^2] [€/kW]	b	Beam	WF	Working Fluid
hr	Hour angle [°]	tot	Total	PP	Pinch point [°C]
R	Radiation tilt factor [-]	inv	Investment	ORC	Organic Rankine Cycle
E	Solar energy [kWh]	h	Horizontal	LCOE	Levelized Cost of Electricity

References

[1] Kalogirou S.A., Solar thermal collectors and applications. Prog Energy Combust Sci 2004;30:231–95.

[2] Karellas S., Roumpedakis T.C., Solar thermal power plants. Solar Hydrogen Production: Processes, Systems and Technologies 2019:179–235.

[3] Tchanche B.F., Lambrinos G., Frangoudakis A., Papadakis G., Low-grade heat conversion into power using organic Rankine cycles – A review of various applications. Renewable and Sustainable Energy Reviews 2011;15:3963–79.

[4] Golonis C., Skiadopoulos A., Manolakos D., Kosmadakis G., Assessment of the performance of a low-temperature Organic Rankine Cycle engine coupled with a concentrating PV-Thermal system. Renew Energy 2021;179:1085–97.

[5] Manolakos D., Kosmadakis G., Kyritsis S., Papadakis G., Identification of behaviour and evaluation of performance of small scale, low-temperature Organic Rankine Cycle system coupled with a RO desalination unit. Energy 2009;34:767–74.

[6] Soulis K.X., Manolakos D., Ntavou E., Kosmadakis G., A geospatial analysis approach for the operational assessment of solar ORC systems. Case study: Performance evaluation of a two-stage solar ORC engine in Greece. Renew Energy 2022;181:116–28.

[7] Roumpedakis T.C., Loumpardis G., Monokrousou E., Braimakis K., Charalampidis A., Karellas S., Exergetic and economic analysis of a solar driven small scale ORC. Renew Energy 2020;157:1008–24.

[8] Schuster A., Karellas S., Aumann R., Efficiency optimization potential in supercritical Organic Rankine Cycles. Energy 2010;35:1033–9.

[9] Smith I.K., Development of the trilateral flash cycle system: Part 1: Fundamental considerations. Proceedings of the Institution of Mechanical Engineers, Part A: Journal of Power and Energy 1993;207:179–94.

[10] Kanno H., Shikazono N., Experimental study on two-phase adiabatic expansion in a reciprocating expander with intake and exhaust processes. Int J Heat Mass Transf 2016;102:1004–11.

[11] Smith I.K., Stošić N., Aldis C.A., Development of the trilateral flash cycle system. Part 3: The design of high-efficiency two-phase screw expanders. Proceedings of the Institution of Mechanical Engineers, Part A: Journal of Power and Energy 1996;210:75–92.

[12] Öhman H., Lundqvist P., Experimental investigation of a Lysholm Turbine operating with superheated, saturated and 2-phase inlet conditions. Appl Therm Eng, vol. 50, Pergamon; 2013, p. 1211–8.

[13] Bianchi G., Kennedy S., Zaher O., Tassou S.A., Miller J., Jouhara H., Numerical modeling of a two-phase twin-screw expander for Trilateral Flash Cycle applications. International Journal of Refrigeration 2018;88:248–59.

[14] Vasuthevan H., Brümmer A., Theoretical investigation of flash vaporisation in a screw expander. IOP Conf Ser Mater Sci Eng, vol. 232, Institute of Physics Publishing; 2017.

[15] Taniguchi H., Kudo K., Giedt W.H., Park I., Kumazawa S., Analytical and experimental investigation of two-phase flow screw expanders for power generation. J Eng Gas Turbine Power 1988;110:628–35.

[16] Skiadopoulos A., van Heule X., Kosmadakis G., Manolakos D., de Paepe M., Lecompte S., Thermodynamic low-order model for the simulation of two-phase expansion within a TFC unit. In: of Munich TU, editor. Proceedings of the 6th International Seminar on ORC Power Systems, Technical University of Munich; 2021.

[17] Baccioli A., Antonelli M., Desideri U., Technical and economic analysis of organic flash regenerative cycles (OFRCs) for low temperature waste heat recovery. Appl Energy 2017;199:69–87.

[18] Lai K.Y., Lee Y.T., Chen M.R., Liu Y.H., Comparison of the trilateral flash cycle and Rankine cycle with organic fluid using the pinch point temperature. Entropy 2019;21.

[19] Bell I.H.,Wronski J., Quoilin S., Lemort V., Pure and pseudo-pure fluid thermophysical property evaluation and the open-source thermophysical property library coolprop. Ind Eng Chem Res 2014;53:2498–508.

[20] Kalogirou S.A., Solar energy engineering: Processes and systems. Solar Energy Engineering: Processes and Systems 2009:1–760.

[21] Tzivanidis C., Bellos E., Antonopoulos K.A., Energetic and financial investigation of a stand-alone solar-thermal Organic Rankine Cycle power plant. Energy Convers Manag 2016;126:421–33.

[22] Braimakis K., Karellas S., Integrated thermoeconomic optimization of standard and regenerative ORC for different heat source types and capacities. Energy 2017;121:570–98.

[23] Quoilin S., Broek M. Van Den, Declaye S., Dewallef P., Lemort V., Techno-economic survey of Organic Rankine Cycle (ORC) systems. Renewable and Sustainable Energy Reviews 2013;22:168–86.

[24] Delgado-Torres A.M., García-Rodríguez L., Analysis and optimization of the low-temperature solar organic Rankine cycle (ORC). Energy Convers Manag 2010;51:2846–56.

https://doi.org/10.52202/069564-0010